Self-Organized Microporous Structures Based on Surfactant-Encapsulated Polyoxometalate Complexes

Hang Sun, Haolong Li, Weifeng Bu, Miao Xu, and Lixin Wu*

Key Laboratory for Supramolecular Structure and Materials of Ministry of Education, Jilin University, Changchun 130012, People's Republic of China

Received: July 18, 2006; In Final Form: October 6, 2006

Self-organized microporous structures based on a series of surfactant-encapsulated polyoxometalate complexes (SECs) have been prepared by using ordered condensed droplets as a template. Among these structures, ordered honeycomb structures were obtained and characterized in detail by taking $(DODA)_{12}H[Eu(SiW_{11}O_{39})_2]$ (SEC-1) as an example. Optical microscope, atomic force microscopic, and scanning electron microscopic measurements confirmed the formation of three-dimensional microporous structure, in which the top surface shows a highly ordered honeycomb structure. As compared to common solvent-casting films, the corresponding honeycomb films are more hydrophobic and possess more ordered lamellar structures. Both the wettability and the size of SECs exert significant influence on the formation of microporous structures. The proper hydrophobicity of SECs was proposed to be an essential factor for the formation of honeycomb films, and large-sized SECs are favorable for the fabrication of highly ordered honeycomb structures. The conditions for the formation of different surface morphologies have been discussed in terms of the contact angle of SECs at the interface between water and chloroform, and a contact angle slightly greater than 90° is found to be a prerequisite for the formation of honeycomb structures. The results reported in this paper not only help to further comprehend the mechanism of the formation of honeycomb structures, but also provide some guidance for the design of ordered microporous films based on organic/inorganic hybrid materials, exemplified by the organic/nanoparticle complexes.

Introduction

Ordered microporous structures based on molecular self-organization have attracted considerable attention over recent years due to their potential applications in diverse areas such as membranes, photonic or optoelectronic devices, and catalysis.[1] A variety of self-assembly or template methods including ordered arrays of colloidal crystals, microphase separation of block copolymers, microemulsions, template-induced self-assemblies of amphiphiles, and so on, have been developed to fabricate ordered structures with submicro- and nanometer scales.[2] However, exploiting new mono-dispersed templates for fabricating ordered porous films, which can be easily removed from a substrate used in the film formation, is still a challenging step. Recently, a facile dynamic template approach that can be applied to prepare highly ordered microporous films with hexagonal array by casting a polymer solution under humid airflow has been reported by Francois and co-workers.[3] The condensed water droplets caused by rapid cooling due to solvent evaporation act as the template that direct the formation of ordered microporous film,[4] and by using this method ordered microporous films have been obtained with a variety of materials such as linear polymers,[5] starlike polymers,[3,6] block copolymers,[7] amphiphilic polymers,[8] conjugated polymers,[9] and even organic/inorganic hybrid complexes.[10] Subsequently, various ordered microporous structures with sizes ranging from 50 nm to 20 μm have been reported, and different functionalities such as superhydrophobic surface,[11] microlens array,[12] cell culture substrate,[13] patterned template, etc., were obtained.[14] Meanwhile, some nanomaterials exhibiting size-dependent functional properties such as Au, Ag, and CdSe nanoparticles are also applied to fabricate highly ordered microporous films,[15] which extend the range of building blocks for pattern formation.

Polyoxometalates (POMs) are intriguing nanosized clusters with a variety of applicable properties in catalysis, optics, and magnetics,[16] and can be modified by cationic surfactants by exchanging their counterions, forming surfactant-encapsulated clusters (SECs) as presented in Figure 1.[17a] Most SECs can be well dissolved in organic solvents and readily processed into thin films by LB technique and solvent-casting method, and can be further incorporated into polymer or liquid crystal systems to fabricate hybrid materials.[17] The amphiphilic character of SECs derived from the coexistence of the hydrophobic alkyl chain shell and the hydrophilic cluster core, as well as their relatively large molecular weights, similar to those of ligand-stabilized nanoparticles,[15] make SECs good candidates for the preparation of microporous films. Indeed, we first found a POM-based honeycomb structure using a special SEC, $(DODA)_4H[Eu(H_2O)_2SiW_{11}O_{39}]$, by casting its solution under humid airflow.[18] However, the nature in the formation of such SECs' microporous films has not been fully revealed, and the influence factors are also unclear, which are important for the fabrication and application of SECs' microporous films. Therefore, a further systematic investigation becomes necessary. Moreover, we can readily adjust the functional properties of SECs by changing the number and length of surfactants as well as the POMs themselves. Consequently, it is possible to understand the role of SECs during the formation of honeycomb-

* Corresponding author. E-mail: wulx@jlu.edu.cn.

10.1021/jp064535b CCC: $33.50
Published on Web 11/18/2006

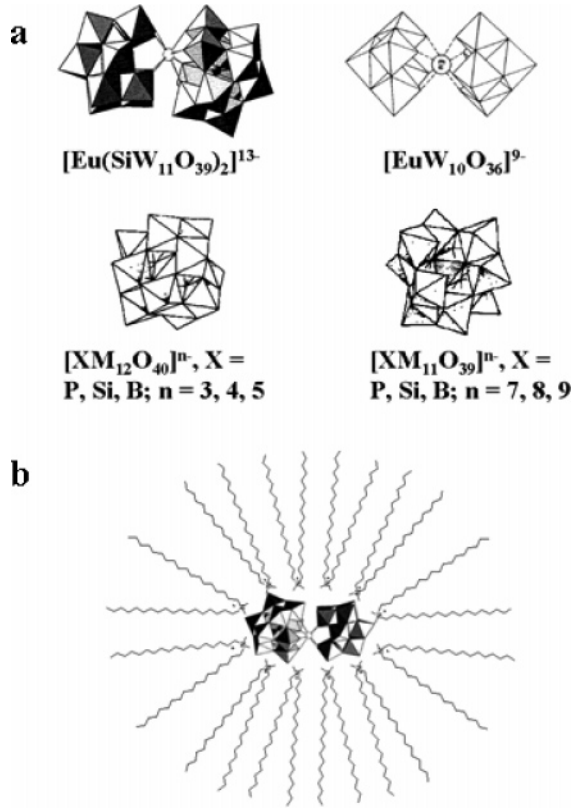

Figure 1. (a) Coordination polyhedral representations of the POMs applied for encapsulation, classified by their different structures; (b) the schematic drawing of the core−shell structure of $(DODA)_{12}H[Eu(SiW_{11}O_{39})_2]$ (SEC-1).

patterned film and to establish a definitive correlation between the SECs' inherent properties and the formed microporous structures.

In this Article, we have systematically investigated the influence of SECs' alkyl chain density, length, and SECs' size on the formation of honeycomb structures. We further discussed and analyzed the conditions under which different surface morphologies were formed in terms of the contact angle of SECs at the interface between water and chloroform. The suitable contact angle was found to be a prerequisite for the formation of honeycomb-patterned films. These results will not only help to optimize the preparation condition of patterned surfaces, but also provide some guidance for the design of microporous films based on POMs with specific functions.

Experimental Section

Materials. POMs, $K_{13}[Eu(SiW_{11}O_{39})_2]\cdot 20H_2O$ (POM-1), $K_5BW_{12}O_{40}$ (POM-4), $K_7PW_{11}O_{39}$ (POM-5), $K_8SiW_{11}O_{39}$ (POM-6), $K_9BW_{11}O_{39}$ (POM-7), and $Na_9[EuW_{10}O_{36}]\cdot 32H_2O$ (POM-8), were freshly prepared according to the literature procedures, respectively.[19] $H_3PW_{12}O_{40}$ (POM-2) and $H_4SiW_{12}O_{40}$ (POM-3) were purchased from SCR and used without further purification. Dimethyl dioctadecylammonium bromide (DODA·Br, 99%) was purchased from Acros Organics and used as received. Dimethyl dihexadecylammonium bromide (DHDA·Br), dimethyl ditetradecylammonium bromide (DTDA·Br), and dimethyl didodecylammonium bromide (DDDA·Br) were synthesized through a modified procedure as reported in the literature.[20]

Preparation of SECs. SECs were synthesized according to the previously reported procedures,[17] exemplified by SEC-1. POM-1 was dissolved in aqueous solution, and then a chloroform solution of DODA·Br was added with stirring. The initial molar ratio of DODA·Br to POM-1 was controlled at 10.5:1. The organic phase was separated, and $(DODA)_{12}H[Eu(SiW_{11}O_{39})_2]$ (SEC-1) was obtained by evaporating the chloroform to dryness. Next, the sample was further dried under vacuum until its weight remained constant. Following similar procedures, $(DODA)_3PW_{12}O_{40}$ (SEC-2), $(DODA)_4SiW_{12}O_{40}$ (SEC-3), $(DODA)_5BW_{12}O_{40}$ (SEC-4), $(DODA)_7PW_{11}O_{39}$ (SEC-5), $(DODA)_8SiW_{11}O_{39}$ (SEC-6), $(DODA)_9BW_{11}O_{39}$ (SEC-7), $(DHDA)_9BW_{11}O_{39}$ (SEC-8), $(DTDA)_9BW_{11}O_{39}$ (SEC-9), $(DDDA)_9BW_{11}O_{39}$ (SEC-10), $(DHDA)_{12}H[Eu(SiW_{11}O_{39})_2]$ (SEC-11), $(DHDA)_9[EuW_{10}O_{36}]$ (SEC-12), and $(DHDA)_7PW_{11}O_{39}$ (SEC-13) were prepared. Coordination polyhedral representations of the POMs used for encapsulation and the schematic drawing of the chemical structure of the SECs illustrated by SEC-1 are shown in Figure 1. The fundamental characterizations of all of the SECs, such as elemental analysis and FT-IR spectra, can be seen in the Supporting Information.

Preparation of Microporous Thin Films. The microporous thin films were prepared by direct casting 10 μL of a chloroform solution of SECs (10 mg/mL) onto glass substrates under a moist airflow at ambient temperature. The humid condition was achieved by bubbling nitrogen gas through a water-filled conical flask, and then the nitrogen gas saturated with water vapor was sent from a nozzle onto the solution surface of SECs. The white thin films covering an area of 1 cm^2 were left behind after the complete evaporation of the solvent and water within 30−60 s. The control experiments without humid airflow have been conducted under ambient atmosphere (relative humidity < 30%), and no microporous structures but only unpatterned flat films were obtained.

Measurements. Fourier transform infrared (FT-IR) spectral measurements were performed on a Bruker IFS66V FT-IR spectrometer equipped with a DGTS detector (32 scans), using KBr pellets, and the spectra were recorded with a resolution of 4 cm^{-1}. Element analysis (C, H, N) was carried out on a Flash EA1112 analyzer from ThermoQuest Italia S.P.A. X-ray diffraction was performed on a Rigaku X-ray diffractometer (D/max rA, using Cu Kα radiation at a wavelength of 1.542 Å), and the data were collected from 0.7° to 10°. The optical photographs were taken with an Olympus BX-51 optical microscope (OM). Atomic force microscopy (AFM) images were carried out with a commercial instrument (Digital Instrument, Nanoscope III, and Dimension 3000) at room temperature in air. Scanning electron microscopy (SEM) images were collected on a JEOL JSM-6700F field emission scanning electron microscope. The contact angles were measured on a Drop Shape Analysis System DSA20 MK2 KRÜSS Edward Keller Ltd. at a temperature of 23 ± 1 °C and humidity of 30 ± 5%. The amount of one droplet of water used for the contact angle measurement was about 1 μL. For the water droplet to suffice to soak the SECs' film surface, the stable static contact angle was measured 5 min later.

Results and Discussion

Characterization of SECs' Honeycomb-Patterned Films. We investigated the structure of SECs' honeycomb-patterned films in detail through OM, AFM, and SEM. Because of the similarity of all of the SECs' honeycomb films concerned, here we took SEC-1 film as an example. The prepared SEC-1 honeycomb-patterned film exhibits bright iridescent colors when observed by naked eyes, which is indicative of the formation of a periodic structure.

The optical micrograph in Figure 2a reveals regular spherical pores covering a large area. The tapping mode AFM image

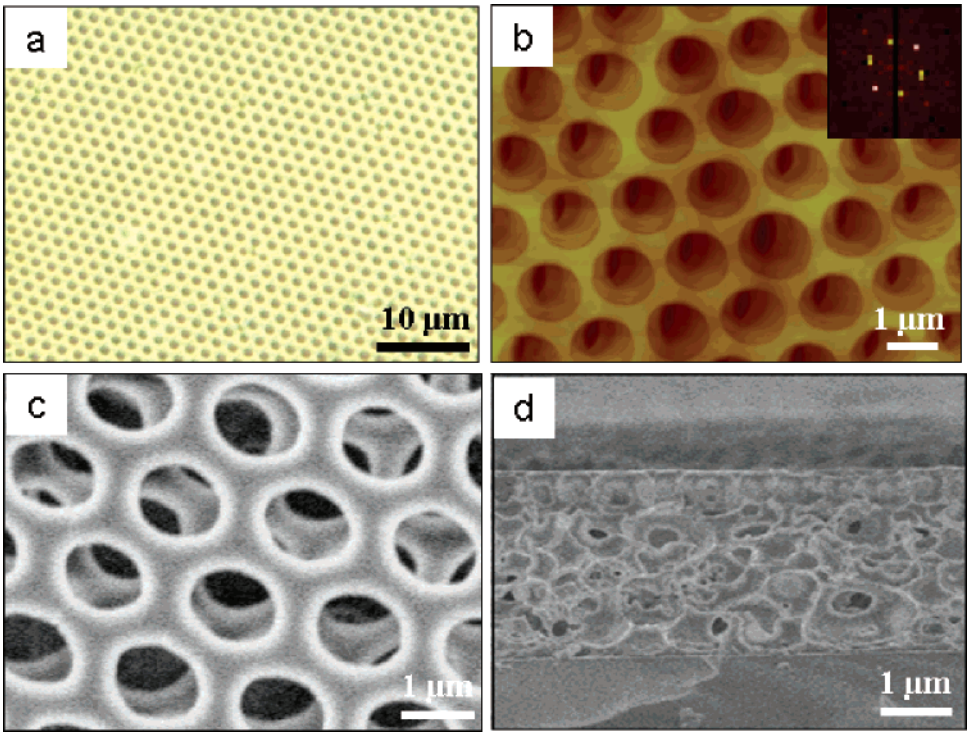

Figure 2. Honeycomb structure images of SEC-1 film: (a) optical micrograph, (b) AFM image and the corresponding FFT pattern (inset b), (c) SEM image of top surface, and (d) SEM image of cross section.

shows an ordered micrometer-sized porous structure with a porous sublayer (Figure 2b). The diameter of the surface pores is 1200 nm, separated by 400 nm. Fast Fourier transform (FFT) pattern (Figure 2b, inset) indicates a hexagonal arrangement of the pores in both the surface layer and the second layer. From the SEM image in Figure 2c, the pores in the second layer, which are relatively ordered, can be seen clearly through the surface layer. The porous structure can be seen in deeper places even at the bottom of the film, whereas the pores in deeper layers become disordered and exhibit a relatively broad size distribution, as seen in the SEM image of the cross section (Figure 2d). Therefore, the microporous film we obtained must be a multilayer structure.

Although multilayer stacking of pores in three-dimension is an interesting phenomenon, the corresponding formation mechanism has not been systematically investigated due to the complexity of influence factors and limited measurements. Srinivasarao and co-workers have shown that the formation of multilayer structures arises from the consecutive sinking of condensed water droplets into the sample solution.[4a] The formation of mono- and multilayer structures was proposed to depend on the solvent density, and multilayer structures were usually found from the solvents with densities lower than that of water. However, in some cases, the multilayer structures have also been observed from carbon disulfide and chloroform with densities higher than that of water.[3a,6,7b,15b] Thus, other factors that may influence the formation of multilayer structures should also exist. Very recently, Bolognesi and co-workers proposed a model to predict and explain the mono- and multilayer structures based on surface and interfacial tensions as well as the sinking of the micrometric water droplets in the solution layer. The prediction can be made by the interfacial energy balance parameter $z_o = (\gamma_w - \gamma_{w/s})/\gamma_s$, where γ_w and γ_s are the surface tensions of water and solution, respectively, and $\gamma_{w/s}$ is the interfacial tension between water and solution.[21a] The calculated z_o for chloroform is equal to 1.63,[21b,22] just fitting the condition of the multilayer stacking of condensed water droplets. Thus, chloroform is believed to be a suitable solvent for the fabrication of multilayer porous films according to the interfacial energy balance parameter. In addition, the proper evaporation speed of chloroform makes the condensed water droplets have enough time to interact with one another, and thus a multilayer stacking of condensed water droplets is allowed.

Besides the solvent, the properties of SEC-1 itself should also be considered. Normally, the density of the solution will change accompanied with the solvent evaporation, which may affect the deposition of water droplets on the film surface. It is difficult for the water droplets to sink into the concentrated solution when the density of the solute is high. So, following the discussion of surface tension, we should analyze the influence of SEC-1 density on the formation of multilayer structure during the chloroform evaporation. The density of SEC-1 can be estimated to be 1.486 g/mL by dividing the molecular weight of SEC-1 by the volume of SEC-1, in which the SEC-1 volume is obtained by summing up the volumes of POM-1 and 12 DODAs.[21c] The calculated density of SEC-1 is almost the same as that of chloroform (1.489 g/mL). Therefore, although SEC-1 contains a POM core, the density of SEC-1 is relatively low due to the high content of hydrocarbon component. Recent literature reported the density of a SEC that has a structure similar to that of SEC-1.[21d] The theoretical crystalline density of $[SiMo_{12}O_{40}]$-$[CTA]_4$ (CTA: cetyltrimethylammonium) is 1.813 g/mL, in which the content of hydrocarbon component is 38%. In the case of SEC-1, the content of hydrocarbon component increases to 55%. Therefore, the density of SEC-1 should be lower, and thus the calculated density of SEC-1 should be reasonable. Because of almost the same density of the solute and solvent, the density of SEC-1 solution should change very little during chloroform evaporation, which helps the water droplets continuously sink into the concentrated solution of SEC-1 during the evaporation. Moreover, the amphiphilic character of SEC-1 can decrease the surface tension of its chloroform solution, which is favorable for the sinking of water droplets. Also, the

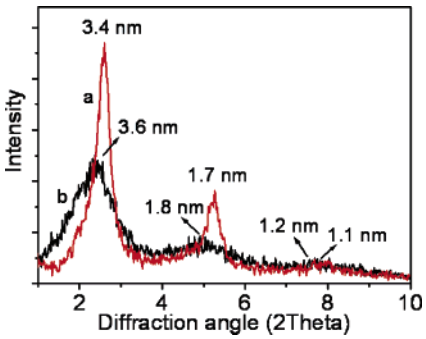

Figure 3. X-ray diffraction patterns of SEC-1 solvent-casting films in the low angle region under (a) the humid condition and (b) laboratory condition (relatively dry condition).

condensed water droplets can be stabilized by SEC-1 even after their sinking into the solution. This also helps to form multilayer microporous structure.

In addition, the different surface morphologies of two kinds of solvent-casting films prepared with and without moisture lead to different surface wettabilities. As compared to the common solvent-casting film of SEC-1 with the water contact angle of 104°, the honeycomb film exhibits a dramatically improved hydrophobicity, and its water contact angle reaches 141°. This is due to the high surface roughness of the microporous morphology, which is favorable for enhancing surface hydrophobicity. We have found the concentration-dependent pattern formation of SEC-1. The honeycomb structures with different surface morphologies were prepared by varying the concentration of SEC-1 from 10 to 0.5 mg/mL (see the Supporting Information). At high concentration, the shape of the pores on film surface is round because the driving force mainly derives from the interfacial tension between water and solution.[7a,8b] Yet in the case of low concentration, the repulsion of the water droplets becomes the main driving force, and thus the shape of the pores is mainly determined by the arrangement of the water droplets. So, the hexagonal structure forms under this condition and the vertex of the hexagon is slightly higher than the other part of the cavity rim due to the tight packing of water droplets.

X-ray diffraction measurements demonstrate that both honeycomb-patterned and common solvent-casting films possess lamellar structures. As seen in Figure 3, the honeycomb-patterned film of SEC-1 shows three Bragg diffraction peaks at 2.59°, 5.23°, and 7.83°, corresponding to the spacings of 3.4, 1.7, and 1.1 nm, respectively. The ratio of the three spacings suggests a lamellar structure with a layer spacing of 3.4 nm. Similar Bragg diffractions are also observed in the common solvent-casting film of SEC-1 but with a little longer layer spacing of 3.6 nm. According to our previous report,[17c] combining the short-axis diameter of POM-1, DODA alkyl chain length, and packing tilt angle, the total thickness of a single layer of SEC-1 could be estimated to be 4.9 nm. Therefore, the alkyl chains of SEC-1 in both films are proposed to have an interdigitated structure with the interdigitated length of 1.5 nm for the honeycomb-patterned film and 1.3 nm for the common solvent-casting film. The deeper interdigitation should be caused by the repulsion between SEC-1 and water. Because of the presence of water droplets, the hydrophobic interaction between the alkyl chains of SEC-1 tends to increase, which decreases the interfacial energy and results in a deeper interdigitated structure. Furthermore, the Bragg diffraction peaks of the honeycomb-patterned film exhibit higher intensity and narrower full-width at half-maximum as compared to those of the common solvent-casting film prepared by casting the same volume of the sample solution. This suggests that the honeycomb-structured film has a more ordered lamellar structure due to the inducement of the water droplets.

The honeycomb-patterned films based on polymers and nanoparticle materials by using ordered condensed droplets as template have been extensively investigated.[4] Considering the consistency of our results with those of polymer systems and modified nanoparticles, a similar mechanism for the formation of highly ordered SECs' honeycomb-patterned films is proposed: (1) When the moist air blows over the SECs' solution surface, the rapid evaporation of chloroform leads to a cooling of the solution surface, and the water vapor condenses onto the solution surface as the temperature falls below its dew point. (2) The water droplets grow by molecular condensation until they reach a self-limiting narrow size distribution and ultimately organize into a hexagonally close-packed lattice at high surface coverage based on the principle of the lowest free energy. (3) Interfacially active SECs adsorb and precipitate at the interface between solution and water droplets to prevent the condensed water droplets from coalescing. The water droplets may continuously sink into the solution. Also, once the surface is free, subsequent water droplets condense and arrange repeatedly, thus forming a multilayer microporous film. (4) After the organic solvent evaporates completely, the water droplets are immobilized in the film and the encapsulated water droplets subsequently evaporate off, leaving behind a three-dimensional microporous film.

Alkyl Chain Density Effect on SECs' Honeycomb-Patterned Films. Because the condensed water droplets act as the template to direct the formation of honeycomb structures, the crucial point for preparing a highly ordered honeycomb structure is to stabilize the water droplets. Thus, for pattern formation it is necessary to develop the SECs with proper interfacial activity, which can adsorb and precipitate at the solvent−water interface to stabilize the water droplet template. It is known that the modified nanoparticles, similar to SECs in our case, stabilize the water droplet template by microphase segregation at the solvent−water interface, which is related to the particle wettability.[23] The wettability of the particles at the solvent−water interface could be quantified by the corresponding interfacial contact angle θ_{ws}, which can be calculated according to the modified Young's equation:

$$\theta_{ws} = \cos^{-1}[(\gamma_w \cos \theta_w - \gamma_s \cos \theta_s)/\gamma_{w/s}] \qquad (1)$$

where γ_w and γ_s are the surface tensions of water and solution, respectively, $\gamma_{w/s}$ is the interfacial tension between water and solution, and the static contact angles of water and chloroform (θ_w and θ_s) can be measured on the flat film of nanoparticles, respectively.[15b,22] For the particles with interfacial contact angle less than 90°, most parts of each particle will stay in the aqueous phase, inducing the interfacial curvature of water around oil and stabilizing o/w emulsion; while in the case of interfacial contact angle greater than 90°, most parts of each particle will stay in the oil phase, forming w/o emulsion. However, if the particles are either too hydrophilic or too hydrophobic, they tend to remain dispersed in either the aqueous or the oil phase. Wang and co-workers reported that when the particle size decreases down to the nanometer scale, the thermal movement would become comparable to the interfacial energy, and spatial fluctuations would suffice to remove the nanoparticles staying at the interface to the bulk phase.[24] So only a contact angle close to 90° is considered to allow the nanoparticles to locate at the interface. Considering the structure similarity between ligand-stabilized nanoparticles and SECs, a similar analysis can be applied in the present system. The wettability of SECs is

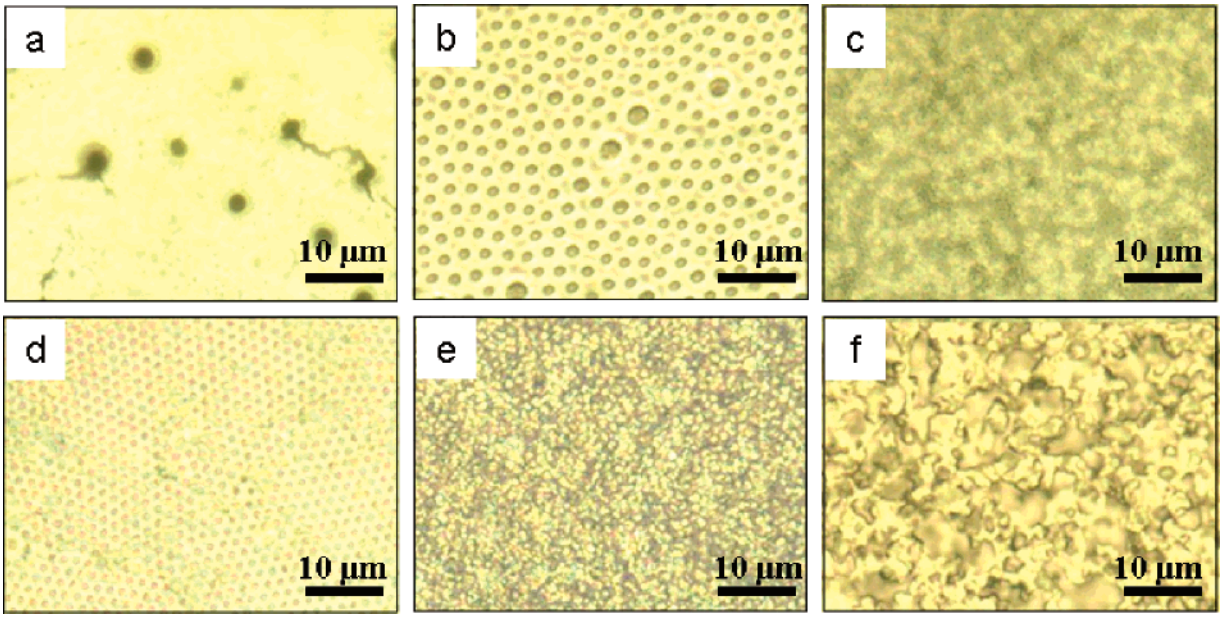

Figure 4. Optical micrographs of patterned surfaces of (a) SEC-2, (b) SEC-3, (c) SEC-4, (d) SEC-5, (e) SEC-6, and (f) SEC-7 films, respectively.

TABLE 1: Surface Area of POMs, Alkyl Chain Number and Density, Measured Water-Stable Static Contact Angle θ_w, and the Corresponding Calculated Contact Angle at the Interface between Water and Chloroform θ_{ws} of SEC-2, SEC-3, SEC-4, SEC-5, SEC-6, and SEC-7, Respectively

	$(DODA)_3PW_{12}O_{40}$ SEC-2	$(DODA)_4SiW_{12}O_{40}$ SEC-3	$(DODA)_5BW_{12}O_{40}$ SEC-4	$(DODA)_7PW_{11}O_{39}$ SEC-5	$(DODA)_8SiW_{11}O_{39}$ SEC-6	$(DODA)_9BW_{11}O_{39}$ SEC-7
surface area of POMs (nm^2)	3.4	3.4	3.4	3.4	3.4	3.4
alkyl chain number	6	8	10	14	16	18
alkyl chain density (nm^{-2})	1.76	2.35	2.94	4.12	4.71	5.29
θ_w (deg) $\pm$ 1°	20	64	70	76	78	95
θ_{ws} (deg)	*a*	80	95	110	115	*a*

[a] It cannot be calculated according to eq 1.

believed to play an important role in the formation of honeycomb structures. Furthermore, combining the condition for forming w/o emulsion and the size of SECs, we predict that an interfacial contact angle of SECs slightly greater than 90° is a prerequisite for the formation of honeycomb microporous structures.

The wettability of SECs could be readily adjusted by changing the alkyl chain number and length of their surfactant components. First, we demonstrate the alkyl chain density effect of SECs on the formation of honeycomb films. We choose a series of anionic POMs with similar geometric structures, but with different negative charges. Among them, POM-2, POM-3, and POM-4 are Keggin heteropolytungstates, and POM-5, POM-6, and POM-7 are the corresponding monolacunary Keggin derivatives, respectively. We encapsulate these POMs with DODA cations to obtain the corresponding complexes, SEC-2, SEC-3, SEC-4, SEC-5, SEC-6, and SEC-7, respectively. These SECs have similar cluster cores, but the number of DODA cations on their surfaces increases from 3 to 9. On the basis of the size of Keggin-type polyoxometalates, the surface area of these POMs should be around 3.4 nm^2. As there are two alkyl chains in each DODA, we estimate the corresponding alkyl chain densities of SECs to be 1.76, 2.35, 2.94, 4.12, 4.71, and 5.29 nm^{-2} by dividing the alkyl chain number by the surface area of the POMs, respectively, as summarized in Table 1.

The wettability of SECs with different alkyl chain densities at the water−solvent interface could be quantified through the corresponding contact angles, and the interfacial contact angles can be calculated according to eq 1 by measuring the contact angles on the flat films of SECs. We measured the water static contact angle and estimated the chloroform static contact angle $\theta_S \approx 0$ for chloroform entirely wets all film surfaces of these SECs. The measured water static contact angles θ_w and the corresponding calculated contact angles θ_{ws} at the interface between water and chloroform are summarized in Table 1.

In the case of SEC-2 with the lowest alky chain density of 1.76, it shows the lowest hydrophobicity. Thus SEC-2 could not stay at the interface between water and solution, but tends to disperse in the aqueous phase when it contacts the condensed water droplets. Consequently, we cannot obtain the θ_{ws} value of SEC-2 by eq 1. As predicted, the disordered pores with a relatively broad size distribution derived from the coagulation of the water droplets were observed everywhere from the corresponding optical micrograph (Figure 4a). For SEC-3 with the alkyl chain density increasing to 2.35, its θ_{ws} value goes up to 80°. It could stay at the interface, but could not stabilize the water droplets in organic solvent. Relatively ordered microporous structure was observed in Figure 4b. Yet the coagulation phenomenon of condensed water droplets still exists, and the size of the pores is obviously larger than that of other SECs' microporous films due to the coagulation.

With the alkyl chain density increasing, the calculated contact angles for SEC-4, SEC-5, and SEC-6 are all greater than 90°. Theoretically speaking, these SECs could stabilize the condensed water droplets, and we have indeed observed microporous structures for all three complexes. In the case of SEC-4, its calculated θ_{ws} value is 95°, only slightly greater than 90°. According to the above analysis, SEC-4 can stay at the interface

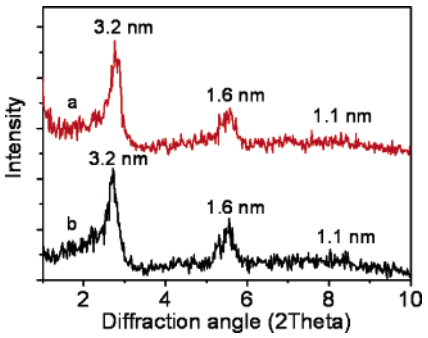

Figure 5. X-ray diffraction patterns of SEC-7 solvent-casting films in the low angle region under (a) the humid condition and (b) laboratory condition (relatively dry condition).

to stabilize the water droplets and prevent them from coalescing most effectively, and thus the size of the stabilized water droplets should be the smallest. Definitely, from Figure 4c and the corresponding SEM image in the Supporting Information, we have clearly observed polydispersed and irregularly arranged small pores with an average diameter of about 200 nm, which are obviously smaller than those of other SECs' microporous films. For SEC-5 with a θ_{ws} value of 110°, it can well stabilize the ordered water droplets and preserve the structure of the microporous film during drying. Thus, an ordered honeycomb structure of SEC-5 is achieved, as seen in Figure 4d. For SEC-6, its θ_{ws} value reaches 115°, much greater than 90°; thus SEC-6 could not stabilize the water droplets effectively, producing poorly ordered microporous film (Figure 4e). Therefore, SECs can be successfully applied to stabilize the water droplets, and proper hydrophobicity is indispensable for the formation of ordered microporous structures.

In the case of SEC-7 with the alkyl chain density of 5.29, it shows the highest hydrophobicity, and its θ_{ws} value cannot be determined by eq 1, which indicates that SEC-7 could not stay at the interface but tends to dissolve in the chloroform phase. Therefore, SEC-7 is not suitable for stabilizing the water droplets. Actually, the corresponding film only shows a disordered surface morphology as seen in Figure 4f. This result is in good agreement with X-ray diffraction data. As has been demonstrated, if the film is prepared under humid airflow, the lamellar structure will be more ordered and have shorter layer spacing induced by the water droplets that sunk into the chloroform solution. The almost identical diffraction patterns for the films prepared with and without humid airflow, as shown in Figure 5, demonstrate that the water droplets cannot be stabilized by SEC-7 and fail to sink into the solution due to the hydrophobicity of SEC-7. Therefore, we have not observed any trace of the condensed water droplets on the film surface of SEC-7 at all, but only a disordered morphology. Thus, high hydrophobicity is not favorable for fabricating SECs' microporous films under the given condition.

In a word, the interfacial contact angle slightly greater than 90° is proved to be a prerequisite for the formation of honeycomb-patterned films, and the appropriate alkyl chain density in SECs for the alkyl chain of octadecyl falls in the range of 2.94−4.71 nm^{-2}. Furthermore, by changing the wettability of the SECs, we can adjust the size and order of the microporous films of SECs.

Alkyl Chain Length and Size Effect on SECs' Honeycomb-Patterned Films. To study the influence of the alky chain length of SECs on the formation of honeycomb film and to further certify that the disordered surface morphology of SEC-7 microporous film results from its high hydrophobicity, we select another three surfactants with structures similar to that of DODA but shorter alkyl chain length, DHDA, DTDA, and DDDA, respectively, to encapsulate the same inorganic core, POM-7. Thus, the hydrophobicity of the resulting complexes (SEC-8, SEC-9, and SEC-10) decreases gradually with the alkyl chain length decreasing, and the morphology change of corresponding SEC films under the same humid condition can be observed.

We measured the water contact angle θ_w and calculated the corresponding contact angle at the water−chloroform interface θ_{ws} for the three SECs as shown in Table 2. In the case of SEC-8, the measured θ_w value is 76°, and the corresponding θ_{ws} value is 110°. The favored contact angle should allow SEC-8 to locate at the interface easily. This complex can stabilize the arranged water droplets by its adsorption and precipitating at the interface, and we did observe the ordered honeycomb structure (Figure 6a). For SEC-9 and SEC-10, the measured θ_w values are 36° and 25°, respectively, and the corresponding θ_{ws} values cannot be calculated from eq 1 with such low measured values. In the case of weak hydrophobic SEC-9, it cannot stay at the interface to stabilize the condensed water droplet array. Also, once the water droplets begin to coagulate, both the droplet size and the polydispersity increase rapidly. Thus, disordered pores with a relatively broad size distribution (Figure 6b) resulting from the coagulation of the condensed water droplets have been observed in a large area. SEC-10 with the lowest hydrophobicity cannot stay at the interface, but tends to dissolve in the aqueous phase when it contacts the condensed water droplets. Consequently, the shape of the water droplets cannot be preserved on the surface of SEC-10 solution at all, and after the solvent and water evaporation, a translucence film with disordered morphology remains (Figure 6c). So, for the given POMs, we can adjust the wettability of the SECs by changing the alkyl chain length on their surface and fabricate ordered honeycomb structures by using SECs with proper hydrophobicity.

It is noted that the stability of nanoparticles adsorbing at the interface between water and solvent relates to the energy of removing the particles from the interface, which dramatically increases with the increasing volume of the particles.[23] Thus, the large-sized particles can stay at the interface more stably and stabilize the ordered water droplet template more efficiently. Consequently, they are more favorable to form ordered honeycomb structure. We believe that such a size effect is also applicable to the present SEC system. To demonstrate this presumption, we selected three different-sized SECs with similar alkyl chain density and the same alkyl chain length, SEC-11, SEC-12, and SEC-13, respectively (Table 3). SEC-11, SEC-12, and SEC-13 were obtained by encapsulating POM-1, POM-8, and POM-5 with DHDA, respectively. POM-5 is a round-shaped mono-lacunary Keggin structure with the volume of 0.59 nm^3. Both POM-8 and POM-1 show an elliptical structure and have the volumes of 0.69 and 1.18 nm^3, respectively. Becaue of the similar structures of DODA and DHDA, the volume of DHDA could be estimated to be 0.89 nm^3 by using the reported DODA volume of 1.03 nm^3 minus the product of DODA lateral area of 0.567 nm^2 and two methylene length of 0.254 nm.[25] Also, the volumes of SECs were obtained by summing up the volumes of DHDA and the corresponding POMs, respectively. The calculated volumes of SEC-11, SEC-12, and SEC-13 are 11.86, 8.70, and 6.82 nm^3, respectively. As seen in Figure 7, the film prepared by SEC-11 with the largest size shows an ordered honeycomb structure, although a few defects appeared. For SEC-12 with middle size, the pores in its microporous film do not show an ordered hexagonal packing, and the film is quite uneven. SEC-13 having the smallest size fails to form a

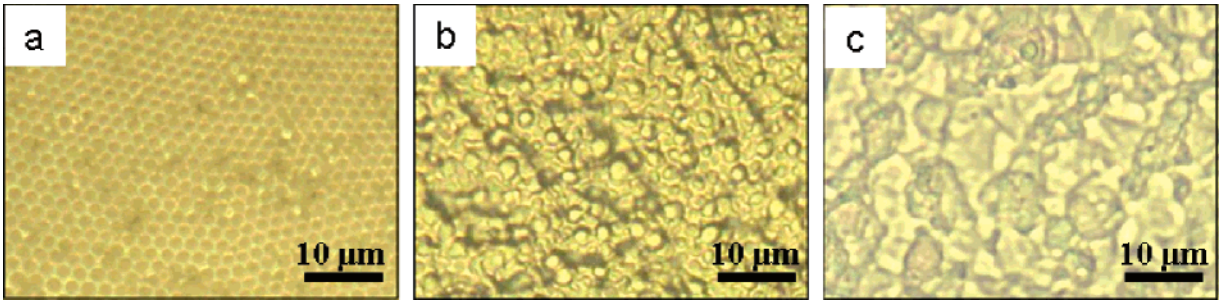

Figure 6. Optical micrographs of patterned surfaces of (a) SEC-8, (b) SEC-9, and (c) SEC-10 films, respectively.

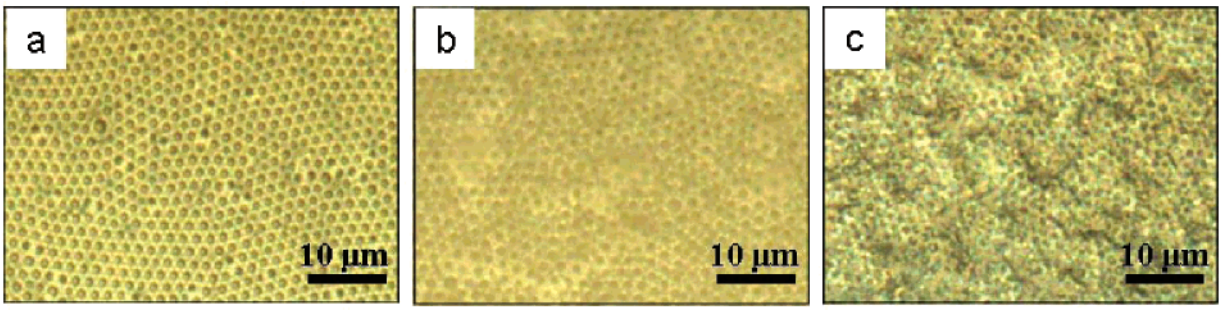

Figure 7. Optical micrographs of patterned surfaces of (a) SEC-11, (b) SEC-12, and (c) SEC-13 films, respectively.

TABLE 2: Measured Water Static Contact Angle θ_w and the Corresponding Calculated Contact Angle at the Interface between Water and Chloroform θ_{ws} of SEC-8, SEC-9, and SEC-10, Respectively

	$(DHDA)_9BW_{11}O_{39}$ SEC-8	$(DTDA)_9BW_{11}O_{39}$ SEC-9	$(DDDA)_9BW_{11}O_{39}$ SEC-10
θ_w (deg) $\pm$ 1°	76	36	25
θ_{ws} (deg)	110	*a*	*a*

[a] It cannot be calculated according to eq 1.

TABLE 3: Surface Area and Volume of POMs, Alkyl Chain Density, and Volume of SEC-11, SEC-12, and SEC-13, Respectively

	$(DHDA)_{12}H[Eu(SiW_{11}O_{39})_2]$ SEC-11	$(DHDA)_9[EuW_{10}O_{36}]$ SEC-12	$(DHDA)_7SiW_{11}O_{39}$ SEC-13
surface area of POMs (nm^2)	6.8	4.8	3.4
alkyl chain density (nm^{-2})	3.53	3.75	4.12
volume of POMs (nm^3)	1.18	0.69	0.59
volume of SECs (nm^3)	11.86	8.70	6.82

honeycomb-patterned film and only presents a disordered microporous structure. In addition, for the complexes encapsulated with DODA instead of DHDA, similar regularity has been observed: the microporous films prepared by large-sized SECs are more ordered than those of small ones. It is noted that the original luminescence of POMs is well retained in its patterned structure of SECs, exemplified by SEC-12, where POM-8 offers the highest luminescent quantum yield among the known luminescent POMs.[17d,f,26]

Conclusions

By using ordered condensed droplets as a template, we demonstrated that general SEC materials can form microporous structure films by their self-organization on solid substrates. Adjusting the hydrophobicity of SECs by changing the alkyl chain density and length, we have successfully prepared the honeycomb-patterned films. Moreover, we found that large-sized SECs help to form highly ordered honeycomb films. The contact angles at the interface between organic solvent and water are found to be responsible for the different morphologies, and the interfacial contact angle slightly greater than 90° is a prerequisite for the formation of honeycomb structure. As compared to common casting films, the honeycomb-patterned films show enhanced hydrophobicity because of the increased roughness resulting from the huge number of surface pores, and more ordered lamellar structures induced by the condensed water droplets. On the basis of the present experimental results, we found the definitive relationship between the inherent properties of SECs and the formed honeycomb structures. This finding is helpful to comprehend the formation mechanism of such microporous structures and provides effective guidance for preparing SEC-based microporous films, which have potential applications in separation membranes, microreactors, and superhydrophobic surfaces. Furthermore, it can also be extended to other relevant fields, especially functional nanoparticle materials, in which the ligands and the nanoparticle cores can be chosen independently.

Acknowledgment. We acknowledge the financial support from the National Natural Science Foundation of China (Grant 20473032), PCSIRT of the Ministry of Education of China (IRT0422), the 111 project (B06009), the Innovation Fund of Jilin University, and the Open Project of State Key Laboratory of Polymer Physics and Chemistry of CAS. We thank Dr. B. Dong from Jilin University and Professor Francois Schue from the University of Montpellier II for their careful correction of

this paper and for helpful discussions. H.L. is thankful for the support of the Graduate Innovation Lab of Jilin University.

Supporting Information Available: Fundamental characterizations of FT-IR spectral and elemental analysis for all of the SECs. Assignment of characteristic infrared spectra of all of the SECs. SEM images of microporous films of SEC-1 for large areas and SEC-4. Optical micrographs of honeycomb films of SEC-1 with the concentrations of 1 and 10 mg/mL. Excitation spectra and emission spectra of SEC-12 porous film. This material is available free of charge via the Internet at http://pubs.acs.org.

References and Notes

(1) (a) Tanev, P. T.; Chibwe, M.; Pinnavaia, T. J. *Nature* **1994**, *368*, 321. (b) Jiang, P.; Hwang, K. S.; Mittleman, D. M.; Bertone, J. F.; Colvin, V. L. *J. Am. Chem. Soc.* **1999**, *121*, 11630. (c) Wijnhoven, J. E. G. J.; Vos, W. L. *Science* **1998**, *281*, 802. (d) Imada, M.; Noda, S.; Chutinan, A.; Tokuda, T.; Murata, M.; Sasaki, G. *Apply. Phys. Lett.* **1999**, *75*, 316. (e) Hulteen, J. C.; Jirage, K. B.; Martin, C. R. *J. Am. Chem. Soc.* **1998**, *120*, 6603.

(2) (a) Velev, O. D.; Jede, T. A.; Lobe, R. F.; Lenhoff, A. M. *Nature* **1997**, *389*, 447. (b) Li, Z.; Zhao, W.; Liu, Y.; Rafailovich, M. H.; Sokolov, J. *J. Am. Chem. Soc.* **1996**, *118*, 10892. (c) Jenekhe, S. A.; Chen, X. L. *Science* **1999**, *283*, 372. (d) Imhof, A.; Pine, D. J. *Nature* **1997**, *389*, 948. (e) Walsh, D.; Mann, S. *Nature* **1995**, *377*, 320. (f) Kresge, C. T.; Leonowicz, M. E.; Roth, W. J.; Vartuli, J. C.; Beck, J. S. *Nature* **1992**, *359*, 710.

(3) (a) Widawski, G.; Rawiso, M.; Francois, B. *Nature* **1994**, *369*, 387. (b) Francois, B.; Pitois, O.; Francois, J. *Adv. Mater.* **1995**, *7*, 1041.

(4) (a) Srinivasarao, M.; Collings, D.; Philips, A.; Patel, S. *Science* **2001**, *292*, 79. (b) Bunz, U. H. F. *Adv. Mater.* **2006**, *18*, 973. (c) Karthaus, O.; Maruyama, N.; Cieren, X.; Shimomura, M.; Hasegawa, H.; Hashimoto, T. *Langmuir* **2000**, *16*, 6071. (d) Pitois, O.; Francois, B. *Eur. Phys. J. B* **1999**, *8*, 225. (e) Maruyama, N.; Koito, T.; Nishida, J.; Sawadaishi, T.; Cieren, X.; Ijiro, K.; Karthaus, O.; Shimomura, M. *Thin Solid Films* **1998**, *327*−*329*, 854.

(5) Peng, J.; Han, Y.; Fu, J.; Yang, Y.; Li, B. *Macromol. Chem. Phys.* **2003**, *204*, 125.

(6) Stenzel-Rosenbaum, M. H.; Davis, T. P.; Fane, A. G.; Chen, V. *Angew. Chem., Int. Ed.* **2001**, *40*, 3428.

(7) (a) Cheng, C. X.; Tian, Y.; Shi, Y. Q.; Tang, R. P.; Xi, F. *Langmuir* **2005**, *21*, 6576. (b) Hayakawa, T.; Horiuchi, S. *Angew. Chem., Int. Ed.* **2003**, *42*, 2285.

(8) (a) Nishikawa, T.; Ookura, R.; Nishida, J.; Arai, K.; Hayashi, J.; Kurono, N.; Sawadaishi, T.; Hara, M.; Shimomura, M. *Langmuir* **2002**, *18*, 5734. (b) Yu, C.; Zhai, J.; Gao, X.; Wan, M.; Jiang, L.; Li, T.; Li, Z. *J. Phys. Chem. B* **2004**, *108*, 4586.

(9) (a) Govor, L. V.; Bashmakov, I. A.; Kiebooms, R.; Dyakonov, V.; Parisi, J. *Adv. Mater.* **2001**, *13*, 588. (b) Song, L.; Bly, R. K.; Wilson, J. N.; Bakbak, S.; Park, J. O.; Srinivasarao, M.; Bunz, U. H. F. *Adv. Mater.* **2004**, *16*, 115.

(10) Karthaus, O.; Cieren, X.; Maruyama, N.; Shimomura, M. *Mater. Sci. Eng., C* **1999**, *10*, 103.

(11) (a) Yabu, H.; Takebayashi, M.; Tanaka, M.; Shimomura, M. *Langmuir* **2005**, *21*, 3235. (b) Yabu, H.; Shimomura, M. *Chem. Mater.* **2005**, *17*, 5231.

(12) Yabu, H.; Shimomura, M. *Langmuir* **2005**, *21*, 1709.

(13) Nishikawa, T.; Nishida, J.; Ookura, R.; Nishimura, S.-I.; Wada, S.; Karino, T.; Shimomura, M. *Mater. Sci. Eng., C* **1999**, *8*−*9*, 495.

(14) de Boer, B.; Stalmach, U.; Nijland, H.; Hadziioannou, G. *Adv. Mater.* **2000**, *12*, 1581.

(15) (a) Yonezawa, T.; Onoue, S.-y.; Kimizuka, N. *Adv. Mater.* **2001**, *13*, 140. (b) Shah, P. S.; Sigman, M. B., Jr.; Stowell, C. A.; Lim, K. T.; Johnston, K. P.; Korgel, B. A. *Adv. Mater.* **2003**, *15*, 971. (c) Böker, A.; Lin, Y.; Chiapperini, K.; Horowitz, R.; Thompson, M.; Carreon, V.; Xu, T.; Abetz, C.; Skaff, H.; Dinsmore, A. D.; Emrick, T.; Russell, T. P. *Nat. Mater.* **2004**, *3*, 302. (d) Li, J.; Peng, J.; Huang, W.; Wu, Y.; Fu, J.; Cong, Y.; Xue, L.; Han, Y. *Langmuir* **2005**, *21*, 2017.

(16) (a) Pope, M. T.; Müller, A. *Angew. Chem., Int. Ed. Engl.* **1991**, *30*, 34. (b) *Chem. Rev.* **1998**, *98*, 1. The entire issue is devoted to polyoxometalates. (c) Pope, M. T.; Müller, A. *Polyoxometalate Chemistry from Topology via Self-Assembly to Application*; Kluwer Academic Publishers: Dordrecht, The Netherlands, 2001.

(17) (a) Faul, C. F. J.; Antonietti, M. *Adv. Mater.* **2003**, *15*, 673. (b) Bu, W.; Fan, H.; Wu, L.; Hou, X.; Hu, C.; Zhang, G.; Zhang, X. *Langmuir* **2002**, *18*, 6398. (c) Bu, W.; Wu, L.; Zhang, X.; Tang, A.-C. *J. Phys. Chem. B* **2003**, *107*, 13425. (d) Bu, W.; Li, H.; Li, W.; Wu, L.; Zhai, C.; Wu, Y. *J. Phys. Chem. B* **2004**, *108*, 12776. (e) Li, W.; Bu, W.; Li, H.; Wu, L.; Li, M. *Chem. Commun.* **2005**, 3785. (f) Li, H.; Qi, W.; Li, W.; Sun, H.; Bu, W.; Wu, L. *Adv. Mater.* **2005**, *17*, 2688.

(18) Bu, W.; Li, H.; Sun, H.; Yin, S.; Wu, L. *J. Am. Chem. Soc.* **2005**, *127*, 8016.

(19) (a) Peacock, R. D.; Weakley, T. J. R. *J. Chem. Soc. A* **1971**, 1836. (b) Weinstock, I. A.; Cowan, J. J.; Barbuzzi, E. M. G.; Zeng, H.; Hill, C. L. *J. Am. Chem. Soc.* **1999**, *121*, 4608. (c) Haraguchi, N.; Okaue, Y.; Isobe, T.; Matsuda, Y. *Inorg. Chem.* **1994**, *33*, 1015. (d) Sugeta, M.; Yamase, T. *Bull. Chem. Soc. Jpn.* **1993**, *66*, 444.

(20) (a) Ueoka, R.; Matsumoto, Y. *J. Org. Chem.* **1984**, *49*, 3774. (b) Okahata, Y.; Ando, R.; Kunitake, T. *Bull Chem. Soc. Jpn.* **1979**, *52*, 3647.

(21) (a) Bolognesi, A.; Mercogliano, C.; Yunus, S.; Civardi, M.; Comoretto, D.; Turturro, A. *Langmuir* **2005**, *21*, 3480. (b) Park, M. S.; Joo, W.; Kim, J. K. *Langmuir* **2006**, *22*, 4594. (c) $\rho_{SEC-1} = 12\ 114.1586$ (molecular weight of SEC-1)/[6.02*10^{23}*(1.03 (volume of DODA)*12 + 1.18 (volume of POM-1))*10^{-21}]. (d) Nyman, M.; Ingersoll, D.; Singh, S.; Bonhomme, F.; Alam, T. M.; Brinker, C. J.; Rodriguez, M. A. *Chem. Mater.* **2005**, *17*, 2885.

(22) Israelachvili, J. N. *Intermolecular and Surface Forces*; Academic Press Inc.: London, 1985; Chapter 14, p 216.

(23) (a) Binks, B. P. *Curr. Opin. Colloid Interface Sci.* **2002**, *7*, 21. (b) Binks, B. P.; Lumsdon, S. O. *Langmuir* **2000**, *16*, 8622. (c) Binks, B. P.; Clint, J. H. *Langmuir* **2002**, *18*, 1270. (d) Lin, Y.; Böker, A.; Skaff, H.; Cookson, D.; Dinsmore, A. D.; Emrick, T.; Russell, T. P. *Langmuir* **2005**, *21*, 191. (e) Binder, W. H. *Angew. Chem., Int. Ed.* **2005**, *44*, 2.

(24) Wang, D.; Duan, H.; Möhwald, H. *Soft Matter* **2005**, *1*, 412.

(25) Okuyama, K.; Soboi, Y.; Iijima, N.; Hirabayashi, K.; Kunitake, T.; Kajiyama, T. *Bull. Chem. Soc. Jpn.* **1988**, *61*, 1485.

(26) (a) Zhang, T.; Spitz, C.; Antonietti, M.; Faul, C. F. J. *Chem.-Eur. J.* **2005**, *11*, 1001. (b) Binnemans, K.; Görller-Walrand, C. *Chem. Rev.* **2002**, *102*, 2303.